C Adsorbed on Ni(111) and Co(0001) Surfaces

Joseph Smerdon, Vincent Fournée, Julian Ledieu, Katariina Pussi

C_{60} adsorbed on Ni(111) and Co(0001) surfaces

Joseph A. Smerdon,*,† Vincent Fournée,‡ Julian Ledieu,‡ and Katariina Pussi¶

†*Centre for Smart Materials and Jeremiah Horrocks Institute for Mathematics, Physics and Astronomy, University of Central Lancashire, Preston, PR1 2HE, United Kingdom*

‡ *Institut Jean Lamour UMR 7198, Université de Lorraine – CNRS, Nancy, France*

¶*Physics Department, School of Engineering Science, LUT University, 53851 Lappeenranta, Finland and Natural Resources Institute Finland (Luke), Production Systems, 00790 Helsinki, Finland*

E-mail: jsmerdon@uclan.ac.uk

Abstract

Carbon-60 molecules were deposited on the fcc Ni(111) surface and, for the first time, the surface of bulk hcp Co(0001) and measured using low-energy electron diffraction and scanning tunneling microscopy. An adlayer with predominantly (4×4) domains is formed in each case. Other domains exemplify chiral epitaxial degeneracy. Annealing produces films with bright and dim molecules, with differing details per substrate. For C_{60} adsorption atop Ni(111), annealing results not only in vacancy formation beneath dim molecules, but also in adatom nucleation below bright molecules.

Introduction

The growth of films of molecules on metallic surfaces is one of the primary means of investigation of nanoscale phenomena. It has wide-ranging implications, for example, in molecular electronics, in which the charge transfer between metal interconnects and semiconducting molecules is not trivial.

Buckminsterfullerene[1] has long been the focus of intense interest in various areas of physics and chemistry research. It is part of the archetypal P3HT-PCBM molecular heterojunction photovoltaic cell, due to its status as a good electron acceptor (an n-type molecule).[2] It can be doped to alter its electronic properties; this has been achieved in several ways. Direct incorporation of metal atoms in the fullerene cage results in endohedral metallofullerenes.[3] Post-deposition of rare-earth atoms onto a C_{60} layer adsorbed on a surface under ultra-high vacuum (UHV) also leads to new states in the electronic structure.[4] Reconstruction of the interface can also result in some charge transfer to the molecules.[5]

Adsorption of C_{60} on metallic surfaces under UHV leads to a multiplicity of interesting behaviors: the reader is referred to reference[6] for an in-depth exploration. In general, C_{60} seems to have a remarkable affinity for metal surfaces and adsorption thereon leads to some reconstruction (with moderate heating applied) in many cases. The reconstruction takes the form of vacancy formation, which is energetically favorable as it increases the coordination of the C_{60} molecules with the surface atoms. This in turn leads to 'bright-and-dim' behavior: molecules may be atop surface vacancies (dim), or not (bright). In a subset of these cases, the vacancies have been observed to diffuse around the superstructure, indicating that the activation energy can be provided at temperatures at or close to 300 K.[7–9] Bright and dim behavior also arises from differences in orientation in adsorbed C_{60} molecules, though in this case the contrast difference is less obvious and is accompanied by differing apparent shapes of the molecules.

The formation of a vacancy and subsequent occupation of the vacancy by a C_{60} molecule increases charge transfer between the C_{60} and the metal surface. This has been shown experimentally and via density functional theory (DFT) calculations to occur for adsorption upon Cu(111),[5,10] Ag(100)[4,11] and Ni(111).[12–14] Atop Cu(111), this behavior has recently been used to construct high-performance molecular rectifiers using the surface-electron-doped C_{60} layer as the metal in a Schottky junction.[15,16]

The observation of this profound modification of the electronic structure of the C_{60} by

interaction with reconstructed transition metal surfaces led to a computational investigation of the potential of a C_{60} film on a magnetic substrate (Ni(111)) as a spin filter.[13] The DOS was found to increase at the Fermi level, consistently with the emerging prevailing behavior of C_{60} atop transition metals. Of importance for spintronics applications, the spin-polarization ratio also increased, improving the magnetoresistance of the system and suggesting the possibility of high-performance spin filters.

Despite the great interest in spintronics and relevant molecular systems, there is little existing research on C_{60} adsorption on ferromagnetic substrates. Most of the useful insights gained into C_{60} interactions with metallic surfaces have been done on close-packed surfaces. Iron, the archetypal ferromagnetic metal, does not have a primary close-packed surface due to its preferred bcc structure, so its usefulness in comparison with the existing literature is limited. Work aimed at ultimately exploiting the useful charge transfer from close-packed surfaces to C_{60} molecules must therefore focus on those ferromagnetic metals that do provide a close-packed surface, such as Co(0001) and Ni(111). Fullerene adsorption atop Ni(111) has been performed and the broader aspects of epitaxy have been described, including a previously unobserved tendency of the substrate steps to grow beneath the adsorbed molecules.[12] More recently, a metastable (7×7) superstructure of C_{60}/Ni(111) was observed.[17] Previous work on Co(0001) has been on a thin film of Co(0001) atop Au(111), in an effort to circumvent the martensitic transformation that occurs in bulk Co.[18]

Molecular growth systems on simple metals generally form domains with several degrees of freedom. These include translational degeneracy, due to molecular superstructure unit cells covering multiples of the substrate unit cell, and rotational degeneracy, which occurs when the orders of rotational symmetry differ between substrate and adsorbate, and is the product of these orders of rotational symmetry.

Finally, chiral degeneracy occurs when there is no plane of reflection symmetry perpendicular to the surface. In the popular Wood's notation, there is reflection symmetry for $R30°$ in hexagonal systems and $R45°$ for square systems; for all others any angle $R \neq 0$ results in

chiral degeneracy.

Here we present a study of adsorption of buckminsterfullerene (C_{60}) on the Co(0001) and Ni(111) surfaces. Both systems show translational and chiral epitaxial degeneracy. Both systems also show evidence of surface reconstruction.

Experimental

The metal samples were prepared via sputtering and annealing cycles. Cobalt undergoes a martensitic transformation between the low-temperature hcp phase and the high-temperature fcc phase at about 695 K. We therefore performed annealing treatments at 600 K. As this was insufficient to fully liberate Ar from the surface, we performed Ar sputtering at 500 eV to reduce the penetration depth of Ar^+ ions. Each cycle consisted of sputtering with ion fluence of 2 μA cm^{-2} for 8 hours with simultaneous annealing to 600 K, followed by sputtering at RT with ion fluence of 20 μA cm^{-2} for 30 mins, followed by a final 30 min anneal to 600 K.

We used the same preparation for Ni(111) but raised the annealing temperature to 1070 K. Annealing temperatures were continuously monitored using a Minolta LAND Cyclops 241 optical pyrometer with emissivity set at 0.1.

The 99.9% pure C_{60} from Alfa Aesar was sublimed from a Pyrex tube by heating the tube to 493 K. Temperatures of source and of sample were monitored using K-type thermocouples. Deposition was performed with the sample at room temperature. Scanning tunneling microscopy (STM) and low-energy electron diffraction (LEED) measurements were performed before and after annealing the films as described below.

The dynamical LEED calculations were performed using the Tensor-LEED program.[19] The relativistic phase shifts were calculated using the phase shift program that is packaged with Tensor-LEED. The agreement between the theory and the experiment was tested using the Pendry R-factor and the error bars quoted are calculated using the Pendry RR-function.

Two different sets of phase shifts were used for Co. At the beginning of the analysis both Debye temperatures were set to 445 K. The $l_{\max}$ value was set to 8 and the imaginary part of inner potential was set to -5.0 eV. Optimization included $z-$coordinates of six topmost Co atoms (6 free parameters). Nonstructural parameters were optimised in the final stages of the analysis to 220 K for the "surface" Co; to 10 for $l_{\max}$ and to 6 eV for imaginary part of inner potential. The real part of the inner potential is independent of energy and was allowed to relax as is normal in LEED analysis (7th free parameter).

Results and discussion

Clean Co(0001) and Ni(111) surfaces: LEED and STM

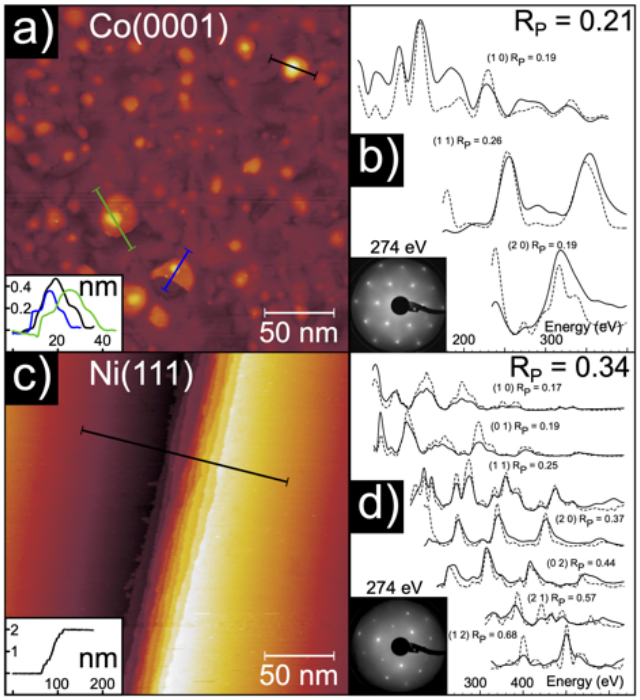

Figure 1: Scanning tunneling microscopy and dynamical low-energy electron diffraction from the clean surfaces of Co(0001) ($I_T = 70$ pA, $V_B = 1.9$ V) and Ni(111) ($I_T = 170$ pA, $V_B = 0.7$ V). a) Co(0001), showing subsurface Ar bubbles and *inset*: profiles taken across islands. b) Dynamical LEED data (solid line) and fit (dotted line) with *inset*: hexagonal pattern at 274 eV. c) Ni(111), showing facetted steps and *inset*: profile across steps, showing step bunching. d) Dynamical LEED data and fit with *inset*: threefold pattern at 274 eV.

Cobalt and nickel are adjacent in the periodic table and have very similar close-packed structures. The primary difference is that Co is composed of ABAB-stacked close-packed layers and Ni is composed of ABC-stacked close-packed layers. The close-packed nearest-neighbor distance (NN) is, for Co, 0.2507 nm, and for Ni, 0.2492 nm.

As mentioned above, Co undergoes a martensitic transformation from hcp (ABAB..) to fcc (ABC..) at 695 K, and a sub-600 K temperature is insufficient to liberate Ar implanted during the sputtering process. Scanning tunneling micrographs therefore show an undulating topography due to the presence of subsurface Ar bubbles as well as the presence of small 1- or 2-layer islands (Figure 1(a)). Repeated preparation cycles serve to flatten the surface in terms of the step/terrace morphology, but the bubbles are never eliminated. A dynamical LEED analysis performed on the clean surface indicates that it remains hcp during our measurements (Figure 1(b)).

Nickel undergoes no such transformation, so high-temperature annealing (1070 K) is possible, resulting in facetted steps and extremely large terraces, as shown via STM in Figure 1(c). A dynamical LEED analysis is also presented in Figure 1(d).

C_{60} atop Co(0001) and Ni(111) surfaces: LEED and STM

Diffraction patterns from C_{60} atop both metals pre- and post-annealing treatments are shown in Figure 2. Fullerene adsorption on both metals at 300 K leads to adoption of a (4×4) structure. Before annealing no other phases are detected with LEED. After annealing at 530 K, both systems develop to show additional phases: (7×7) on Co(0001) and a $R30°$ phase on Ni(111). The (7×7) structure observed on Co(0001) has a C_{60} NN of 1.01 nm, which is very close to the C_{60} bulk value. The intensity of the (4×4) pattern is diminished after annealing C_{60}/Ni(111). This can be attributed to the growth of other domains at the expense of (4×4) domains.

At room temperature, the C_{60} bulk crystal is fcc with a lattice parameter $a = 14.155$ Å, corresponding to a NN of 10.01 Å.[28] The maintenance of a NN close to this value is of

Table 1: C_{60} adsorption structures on close-packed metals. "*B*", when prefixing C_{60}, means "bright".

Substrate	Structure	C_{60}-C_{60} distance (Å)	Vacancy size	Adatom sink location	Reference
Pt(111)	$(2\sqrt{3} \times 2\sqrt{3})R30°$	9.61	1	unknown	[20]
Al(111)	(6×6) (buckled)	9.92	1	*B* C_{60}	[21]
Ni(111)	(4×4)	9.97	7	step+*B* C_{60}	this work, [12,13,17]
Au(111)	$(2\sqrt{3} \times 2\sqrt{3})R30°$	9.99	1	unknown	[9,22]
Pt(111)	$(\sqrt{13} \times \sqrt{13})R13.9°$	9.99	1	unknown	[23]
Graphite	Incommensurate	9.99±0.01	-	-	[24]
Au(111)	$(\sqrt{589} \times \sqrt{589})R14.5°$	10.00	-	-	[25]
Ag(111)	$(2\sqrt{3} \times 2\sqrt{3})R30°$	10.01	1	interstitial	[22,26]
Pb(111)	$(\sqrt{172} \times \sqrt{172})R7.59°$	10.02	-	-	[24]
Co(0001)	(4×4)	10.02	7	unknown	this work
Co/Au(111)	(4×4)	10.02	7	unknown	[18]
Ni(111)	(7×7)	10.07	-	step	[17]
Co(0001)	(7×7)	10.13	-	-	this work
Ni(111)	$(\sqrt{67} \times \sqrt{67})R12.2°$	10.20	-	-	this work
Cu(111)	(4×4)	10.22	7	step	[10]
Co(0001)	$(\sqrt{67} \times \sqrt{67})R12.2°$	10.26	-	-	this work
Cd(0001)	$(2\sqrt{3} \times 2\sqrt{3})R30°$	10.30	-	-	[27]
Au(111)	(7×7)	11.65	-	-	[9]

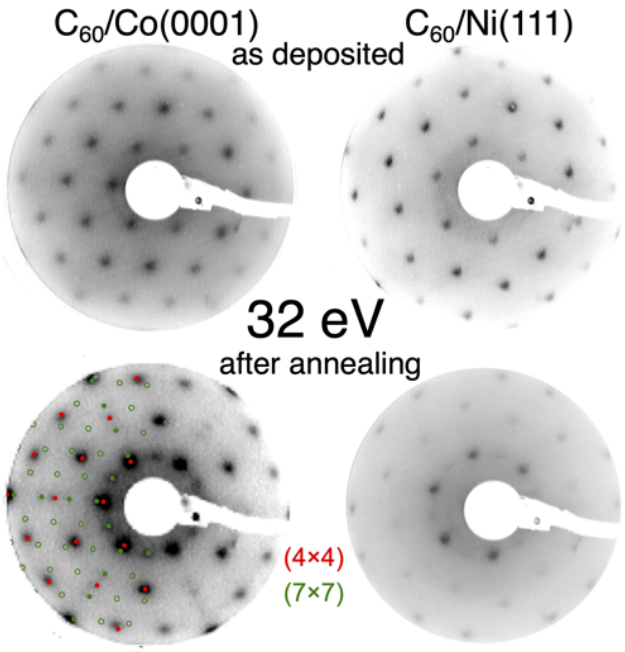

Figure 2: LEED patterns from C_{60}/Co(0001) and C_{60}/Ni(111) before and after annealing. Both show at least one additional phase present after annealing. The green pattern indicates a (7×7) superstructure; filled/empty circles show where corresponding diffraction peaks are/are not observed.

paramount importance in adsorption systems, leading to a rich variety of observed phases, summarised in Table 1. The NN of most close-packed metal surfaces is within the 2.4-2.6 Å range, meaning that a (4×4) superlattice, with 1 molecule in the unit cell, is often observed. However, allowing for more than 1 molecule in the unit cell, and for domain rotation relative to the substrate surface, leads to a densely populated phase diagram for adsorption. The phases with more than 1 molecule per unit cell are termed *higher order commensurate* (HOC) phases.

Li *et al.* adopted a systematic approach called the "hexagonal number sequence" method, proposed by Tkatchenko,[29] to explore C_{60} adsorption atop Pb(111). Here, we use the same method to identify possible adsorption structures for C_{60} atop Co(0001) and Ni(111).

The substrate surface lattice vectors are represented by $\vec{a_1} = (1, 0)a$ and $\vec{a_2} = (1/2, \sqrt{3}/2)a$, where a is the surface NN. Any lattice point at the surface can then be described as a linear combination of these primitive vectors, $\vec{R} = m\vec{a_1} + n\vec{a_2}$, where m and n are integers.

The lattice vectors of a commensurate or HOC layer on this substrate can be described by the lattice vectors $\vec{A_1}$ and $\vec{A_2} = \begin{pmatrix} 1/2 & -\sqrt{3}/2 \\ \sqrt{3}/2 & 1/2 \end{pmatrix} \vec{A_1}$, where $\vec{A_1}$ and $\vec{A_2}$ satisfy $m_0\vec{A_1} + n_0\vec{A_2} = m\vec{a_1} + n\vec{a_2}$, where m, n, m_0 and n_0 are all integers. Each combination of m, n, m_0, n_0 represents a different commensurate or HOC structure and possesses a different lattice parameter and rotation angle. For further description of this technique the reader is referred to Li *et al.*[24]

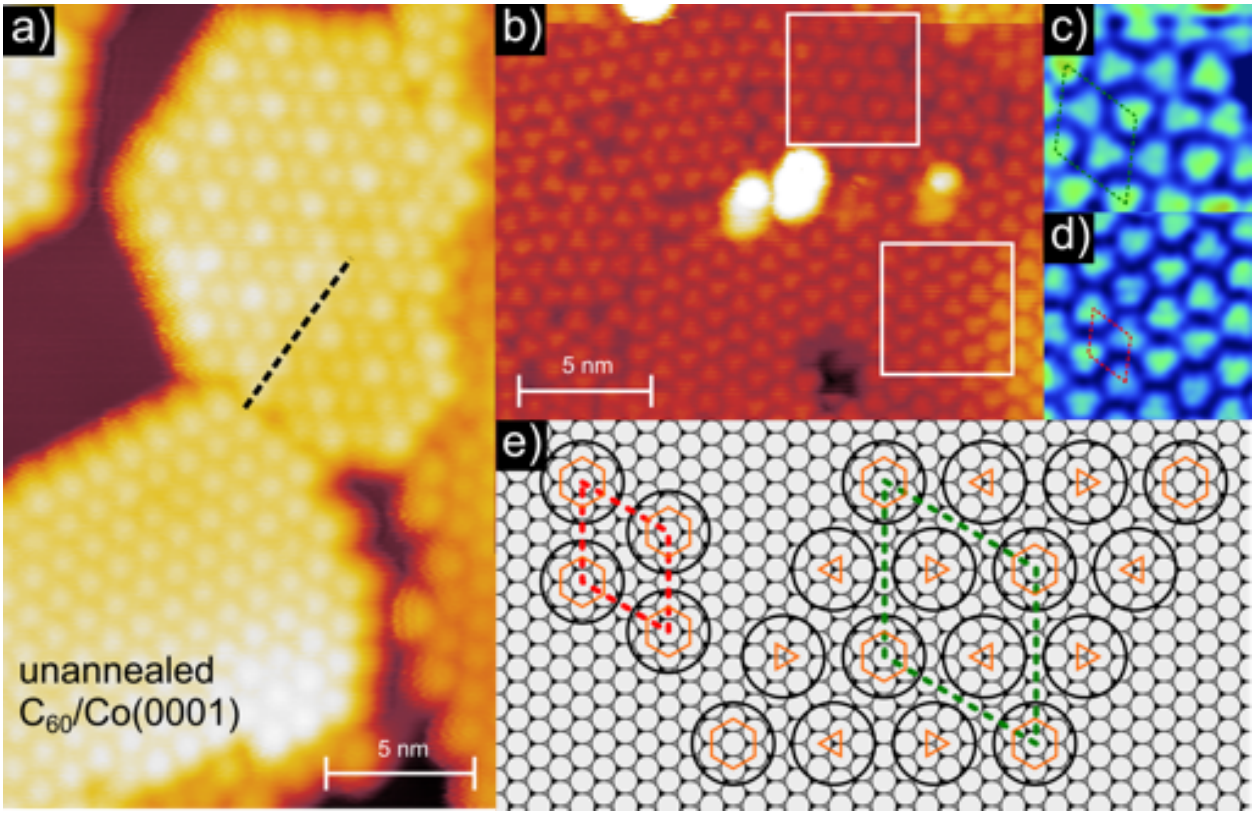

Figure 3: (a) STM topograph of submonolayer domains of C_{60} atop Co(0001) (I_T = 100 pA, V_B = 1 V). The dotted line indicates a screw dislocation running through a (7×7) domain. (b) Another location in the film showing (7×7) and (4×4) domains (I_T = 70 pA, V_B = 2 V). (c,d) Fourier-filtered details of (b), with a high-contrast color scale, showing the orientations of molecules, with unit cells indicated. (e) Structural models of the observed phases. The orange motifs indicate the atoms in the substrate that determine the orientation of the C_{60} molecules. For atop sites, the 6-fold environment leads to 2-fold degeneracy, for hollow sites, the 3-fold environment leads to a single orientation. The orange triangles are inverted compared to the three-fold appearance in STM because the indicated atoms bond to the underside of the C_{60} molecules whereas we see the topside.

As well as the domain orientation of the molecules, there is also the individual molecule orientation to consider. C_{60} is composed of hexagonal and pentagonal facets, with the LUMO

localized around pentagonal facets. Symmetry arguments lead to the conclusion that a molecule presenting with a three-fold or triangular appearance has a hexagonal facet upward. Knowledge of the LUMO shape leads to the conclusion that the three bright spots are edge-on observations of pentagonal facets adjoining the upward hexagonal facet. Therefore, on the opposite side of the molecule, which is in contact with the substrate, there is a hexagonal facet with an oppositely-pointing arrangement of adjoining pentagonal facets.

Atomic resolution of metallic substrates can be difficult or impossible to achieve with STM. For this reason, adsorption sites are usually ascertained via indirect means, such as tip-induced manipulation of molecules,[30] complementary methods such as density functional theory (DFT) or geometric arguments. In the cases under discussion, observations of the STM topographs allow us to use the geometry of the system to unambiguously assign adsorption sites to most C_{60} molecules.

In Figure 3 (a), we present data collected from the Co(0001)–3C_{60}(7×7) (top) and the Co(0001)–C_{60}(4×4) (bottom) phases. Brighter molecules in the domain at the top of (a) indicate the unit cell of the superstructure. High-resolution measurements in (b), enhanced with Fourier filtering and a high-contrast color scale in the details indicated in (c,d) show that the differentiation in molecules seen in (a) originates in the adsorption sites, rather than the individual molecule orientations, which are all hexagon-up. As shown in (e), the atop sites, indicated by orange hexagons and occupied by brighter molecules, are 6-fold, which leads to 2-fold degeneracy in the molecular azimuthal orientation. The hollow sites (orange triangles) are 3-fold and not degenerate, so the molecules at these sites have consistent alternating orientations. The dotted line in (a) indicates a substrate screw dislocation; the domains either side have a relative displacement of 1 C_{60} NN, consistent with the substrate stacking.

We find that most of the C_{60} molecules adsorbed on Co(0001) adopt a (4×4) structure, resulting in a theoretical $NN = 10.028$ Å. As mentioned, results from LEED (Figure 2) indicate an additional phase: (7×7)–3C_{60}(10.13 Å). As can be seen in Figure 3(e), the unit

cells of both the (4×4) phase (red) and the (7×7)–$3C_{60}$ phase (green) have a common orientation. However, because the (7×7)–$3C_{60}$ unit cell contains 3 C_{60} molecules, the C_{60} nearest neighbor directions are perpendicular to the (4×4) NN directions and thus the substrate NN directions.

Results from STM (Figure 3(d)) show that the molecules in the (4×4) phase show 2-fold degeneracy. We therefore conclude that they are adsorbed in atop sites as explained below. In other studies, for C_{60} adsorbed on Cu(111), where the molecules reside in three-fold hollow sites, there is no such degeneracy;[5,15] all molecules in a domain have the same orientation.

In Figure 4 we present STM data from both unannealed systems showing the existence of domains with different azimuthal relationships with the substrate (i.e., $R \neq 0°, 30°$). As mentioned in the Introduction, for hexagonal systems, azimuthal angles $R \neq 0°, 30°$ lead to chiral degeneracy. We directly observe this in Figure 4 (a), which shows several domains of C_{60}/Co(0001), including two $R12°$ domains consistent with a $\sqrt{67}$ phase, one in one chiral orientation and the other in its mirror image.

In Figure 4 (b) we show several domains of C_{60}/Ni(111). The azimuthal orientation of the lower right domain is consistent with a $\sqrt{67}$ structure. The azimuthal orientation of the upper left domain is compatible with several HOC structures.

Annealed films

Bright/dim behavior has been observed in most C_{60} adsorption systems to date, either with or without annealing. We find the same for both systems under discussion, though with clear differences in the details. Unlike the case for C_{60}/Ag(111), we do not find significant evidence of a dependence of dynamic bright/dim behavior on temperature, for either system.

Vacancies

Molecular orientation can play some role in the apparent height of a C_{60} molecule. However, for bright/dim behavior observed on metal surfaces, the height difference is often greater

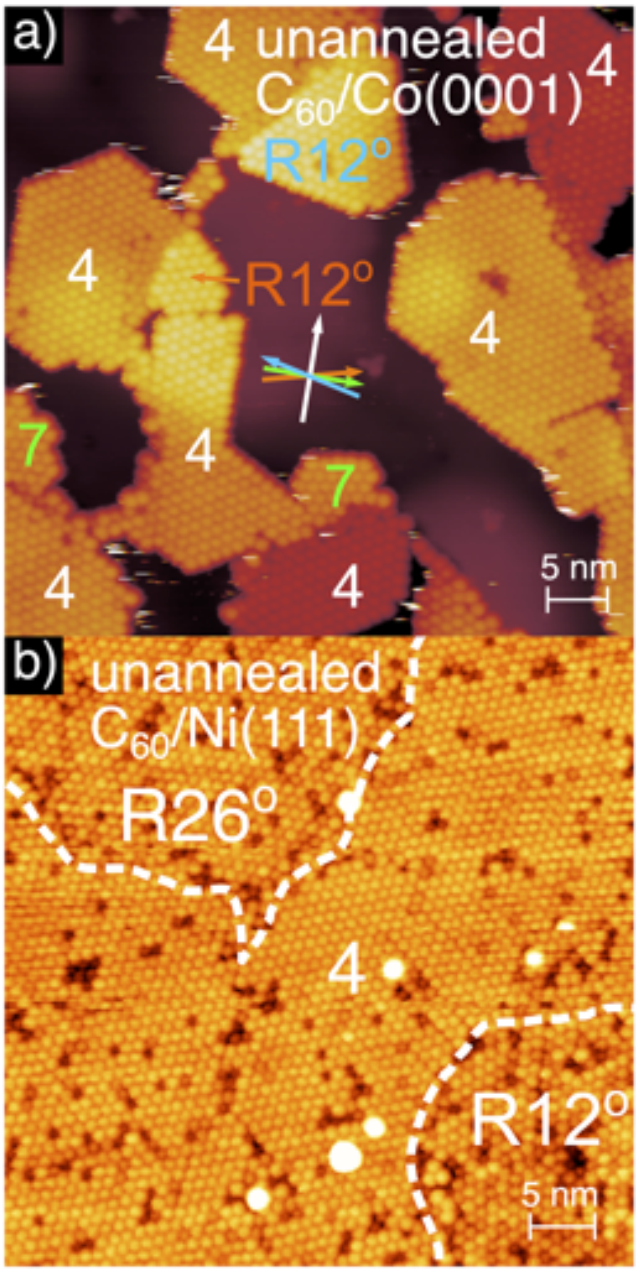

Figure 4: a) STM image of C_{60} atop Co(0001), showing several (4×4) domains, 2 (7×7) domains and both chiralities of $R \pm 12°$ islands ($I_T = 200$ pA, $V_B = 1$ V). Domain NN directions are indicated by appropriately colored arrows. b) STM image of C_{60} atop Ni(111), showing a large central (4×4) domain, a rotated domain in the upper left, and a $R \pm 12°$ domain in the lower right ($I_T = 70$ pA, $V_B = 2$ V).

than can be explained by different molecular orientations – and often, the orientation can be directly observed to be identical, suggesting that the height difference is topographical in origin. In these cases, bright/dim behavior is the result of reconstruction of the substrate surface to form vacancies beneath C_{60} molecules. Such vacancies increase the coordination and hence adsorption energy of the molecules. The increase in adsorption energy counterbalances the energy of formation of a vacancy. There is an activation energy associated with the reconstruction, which is supplied by moderate annealing of the film.

For vacancies on fcc(111) or hcp(0001) surfaces to be symmetrical, and thus ordered, they must all be the same, with the same symmetry as the substrate. This leads to possible candidate vacancy structures for hexagonal systems of 1-atom, 3-atom (triangle) or 7-atom (centered hexagon). 1-atom and 7-atom vacancies are observed in experiments, as recorded in Table 1. 3-atom vacancies have not been observed. It should be noted that, as identical adsorption sites are not directly above each other in consecutive substrate planes, the formation of a 1-atom or 7-atom vacancy removes an atop site and replaces it with a hollow site. If the film prefers hollow site adsorption, there will be a resultant small lateral shift between the B (bright) molecules and the D (dim) molecules, as each will occupy hollow sites on different layers. The creation of vacancies is a source of adatoms, which must relocate somewhere. The three possible sinks for these adatoms are below B molecules, at sites interstitial to C_{60} and at substrate step edges. For annealed C_{60}/Cu(111), 7-atom vacancy formation results in large numbers of adatoms, which migrate to step edges, forming straight, facetted steps.[10,31] Atop Ag(111), a dynamical LEED study found 1-atom vacancy formation, with a possible sink being the interstitial sites between C_{60} molecules,[26] though this is unconfirmed as it has a minimal effect on the LEED data. Atop Al(111), the prevailing interpretation of the buckled (6×6) structure seen via STM is that two out of three C_{60} molecules per unit cell sit atop a 1-atom vacancy, with the adatoms residing in the interstitial sites and the third C_{60} sitting atop unreconstructed Al.[21] An earlier study of C_{60}/Ni(111) showed that, for molecules deposited at higher temperature, C_{60} molecules first adsorbed at steps and

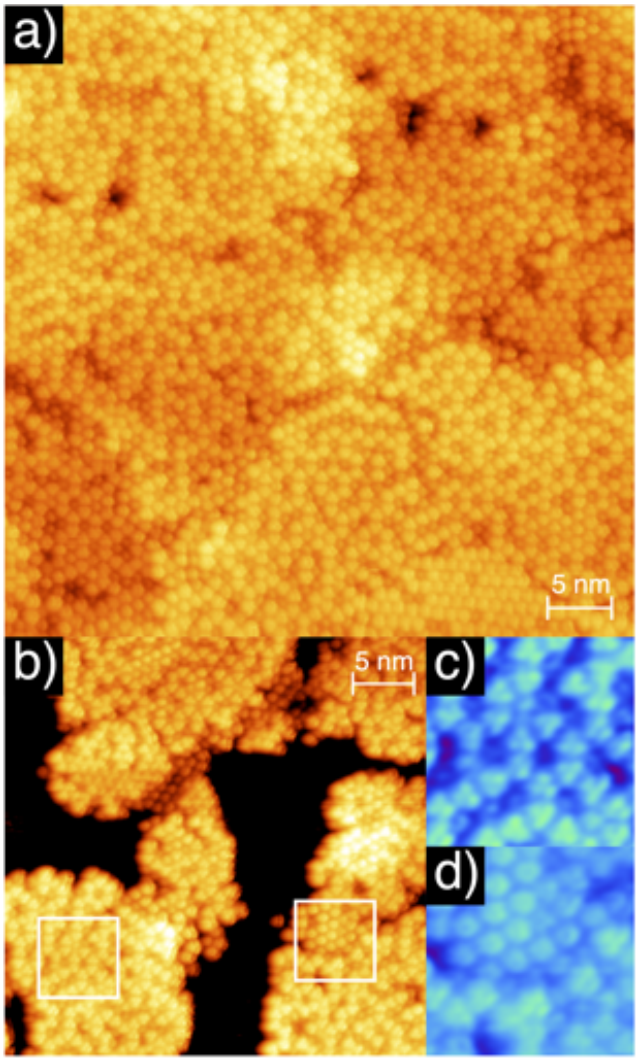

Figure 5: Scanning tunneling micrographs of C_{60}/Co(0001) annealed at 530 K. (a): 50×50 nm image showing the overall $B - D$ structure of the film. A small perpendicular domain is visible in the lower right corner. ($I_T = 190$ pA, $V_B = 2$ V). (b) and (details indicated by white squares) (c-d) High resolution measurements indicating different individual molecular orientations ($I_T = 190$ pA, $V_B = 2$ V).

then adatoms relocated beneath them, causing substrate step growth beneath the adsorbed C_{60}.[12]

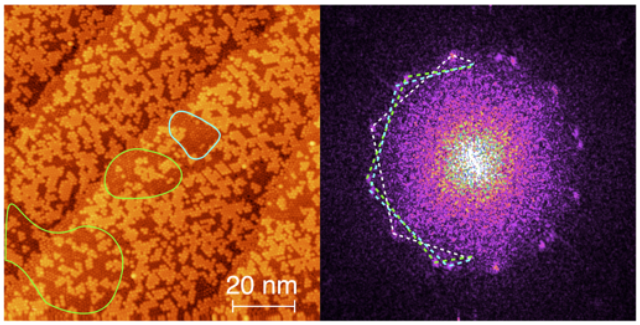

Figure 6: (Left): Micrograph of annealed C_{60}/Ni(111) with (right) associated fast Fourier transform (FFT) (I_T = 100 pA, V_B = 2 V). The relationship between the image and the components of the FFT are indicated with colored shapes. The white hexagon in the FFT indicates the component due to the predominant (4×4) domain orientation.

C_{60}/Co(0001) after 530 K anneal

We show the annealed system in Figure 5. On Co(0001), bright/dim behavior is dependent on the azimuthal orientation of the domain. For the vast majority of material, which is in the (4×4) orientation, most molecules (approximately $^2/_3$) are bright. The undulating nature of the substrate makes it difficult to perform statistical analysis. Many dim molecules are surrounded by 6 bright nearest neighbors, though lines and domains of up to around 12 contiguous dim molecules can be found. The surface includes many screw dislocations that appear to be predominantly occupied by dim molecules. There are also molecules with contrast levels in-between those of the bright and dim molecules. At step edges, it is not clear if the dim molecules of the upper terraces are in the same adsorption geometry as the bright molecules of the lower terrace. Furthermore, this appears to be a stable configuration: extended annealing, or annealing at moderately higher temperatures, does not affect the film morphology or change the relative proportions of B/D molecules.

Most bright molecules have a clear triangular or three-lobed appearance, indicating that they have a hexagonal facet in contact with the substrate. As shown in Figure 5 (c), the orientation appears 2-fold degenerate, suggesting adsorption on atop (6-fold) sites. The

adsorption geometry of dim molecules is less clear, with the orientation of adsorbed molecules not generally available from the data. Some small domains of doughnut-shaped molecules exist, as shown in Figure 5 (d). Following on from the earlier discussion of the LUMO shape, a molecule presenting with a doughnut shape has a pentagonal facet upward (and thus an oppositely-pointing pentagonal facet in contact with the substrate).

The height of three-lobed B molecules is 0.56 ± 0.02 nm, of doughnut B molecules is 0.67 ± 0.05 nm and the height difference between B molecules and D molecules is 0.092 ± 0.007 nm (Supporting Information). This small difference suggests a 1-atom vacancy is formed, rather than a 7-atom vacancy, which would allow the molecule to sit on the layer beneath. There is no significant dependence on bias voltage.

In the much-less observed perpendicularly-oriented material, as in the lower right corner of Figure 5(a), there are far fewer dim molecules. The LEED patterns and apparent NN distance suggest the material is in the (7×7) structure. There is no evidence that the different adsorption sites in the (7×7) unit cell affect the B and D distribution. Also, the superstructure pattern observed in Figure 3(a) is not observed in any data from the annealed film.

It is important to note that these experimental results and interpretations contrast in some important ways with those reported for C_{60} deposited on a thin (7-10 ML) film of Co on Au(111).[18] Kollamana *et al.* performed STM and scanning tunneling spectroscopy (STS) on a submonolayer film of C_{60} on a thin film of Co/Au(111).

Upon deposition at RT, the previous study finds a disordered film. For deposition on a Co crystal, we have found that C_{60} forms ordered islands at RT. A strained surface can modify adsorption potential, which could lead to the disordered growth observed previously. After annealing at 620 K, Kollamana *et al.* observe $R15°$ and $R30°$ domains, along with a majority of $R0°$ domains. Some of the $R0°$ domains have a superstructure similar to the (7×7) superstructure described above, but with inverted contrast. High quality data show the molecular orientation in almost all cases.

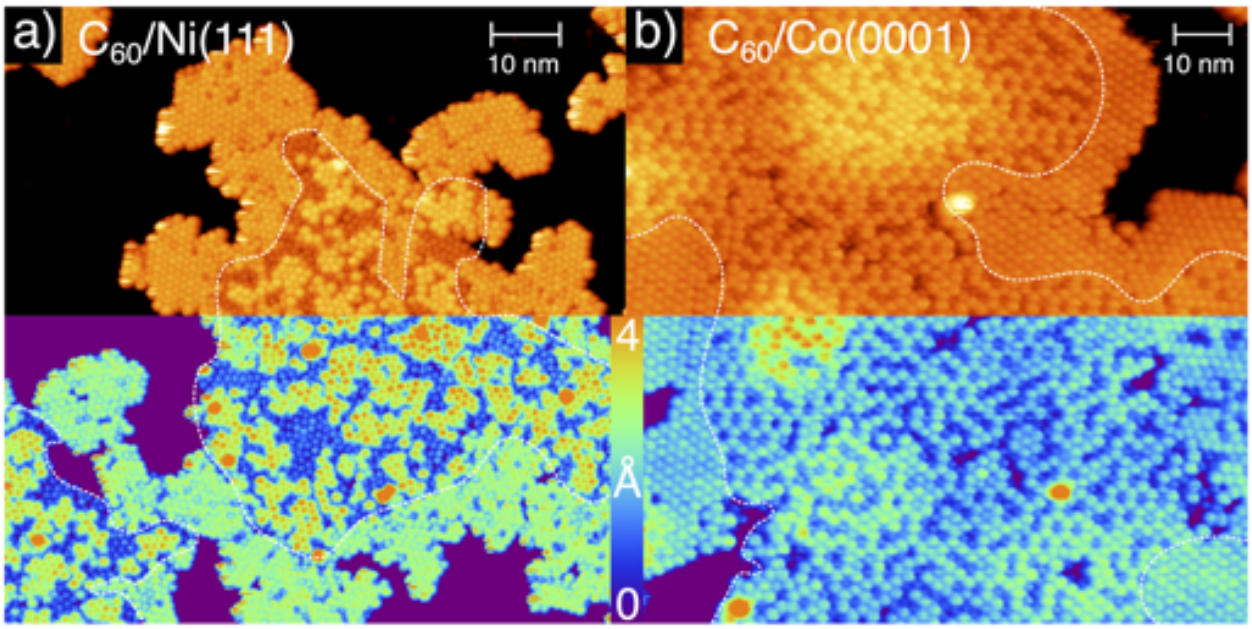

Figure 7: a) C_{60}/Ni(111) (I_T = 50 pA, V_B = −2 V) and b) C_{60}/Co(0001) (I_T = 50 pA, V_B = 2 V) annealed to 530 K with a subsequent additional room-temperature deposition of C_{60}. The boundaries between annealed and unannealed material are shown with white dotted lines. The bottom of each image is recolored with a high-contrast colormap (center: scale bar) to aid identification of differing adsorption situations.

Kollamana *et al.* attribute the formation of the $R15°$ and $R30°$ domains to the presence of a strained Co film with modified lattice constants of 2.77 Å and 2.88 Å. We think this is unlikely, for three main reasons: 1. This represents a strain of between 10%-15%, which may be observed in a pseudomorphic monolayer, but is vanishingly unlikely to persist in a film more than 7 ML thick. The same group has reported that the lattice parameter reverts to the Co bulk value at 7 ML, in a LEED study of the Co film without C_{60} molecules present;[32] 2. In some cases, the domains coexist on the same layer. It is unlikely that different lattice parameters coexist in the same layer of Co, though perhaps not impossible if the Au surface is corrugated beneath the Co surface; 3. A convincing alternative explanation exists, which is that it is very easy for the C_{60} to adopt a HOC structure, as described above for this substrate, and in abundant literature on other substrates.

C_{60}/Ni(111) after 530 K anneal

In Figure 6 we present a large-scale micrograph with associated fast Fourier transform

(FFT). This shows a predominantly (4×4) film with two small domains of differently oriented material. The FFT reveals that these domains are likely to be chirally related, as each domain appears to have an angular offset of the same amount but in opposite directions, relative to substrate NN directions (and therefore to (4×4) domain NN directions). Unlike the case for C_{60}/Co(0001), there appears to be broadly similar $B - D$ behavior independent of domain orientation.

Annealing at 630 K produced surface carbide with the characteristic LEED pattern of the clock reconstruction. For this reason, we did not try annealing at higher temperatures. Therefore, in this study, we did not observe the recently reported (7×7) overlayer structure obtained by annealing at 670 K.[17] This structure is remarkably similar to the (7×7) phase we report above for C_{60}/Co(0001). The identified adsorption sites are identical, with 2 of the C_{60} in the unit cell in alternate threefold sites and the remaining C_{60} in a two-fold degenerate atop site. The difference on Ni(111) is that the 3rd molecule does not decorate all sites, and sits higher than it does on Co(0001), at 0.2 nm above its neighboring molecules. The increased buckling of the film is consistent with the smaller surface NN of Ni compared to Co. Picone *et al.* suggest that the increased buckling may be attributable to Ni adatoms beneath the C_{60}, similar to the case for C_{60} atop Al(111).

In Figure 7, we emulate the experiment conducted by Pai *et al.* on C_{60}/Cu(111)[10] to compare annealed and unannealed films. In this experiment, C_{60} is deposited on the substrate to submonolayer coverage and then annealed, activating the $B-D$ reconstruction. Following this, more C_{60} is deposited, at room temperature. This additional C_{60} agglomerates around the existing islands, leading to a *core-shell* island morphology. Molecules in the core sit atop reconstructed substrate and molecules in the shell sit atop unreconstructed substrate. In this way a direct comparison is provided between molecules in pre- and post-annealed situations. For adsorption on Cu(111), the reconstruction is total, meaning core molecules are all atop 7-atom vacancies – i.e., all D. In the present studies, the reconstructions are self-limiting and core molecules are a mix of B and D.

In Figure 7 (a), we investigate the C_{60}/Ni(111) film. At least three distinct substrate-adsorbate relationships are present. In the lower half, the differentiation is clear: annealed molecules are orange (B) or blue (D). C_{60} molecules deposited at room temperature are green. Measurements of the height histogram indicate 0.26 ± 0.01 nm height difference between annealed B and D molecules, and a 0.08 ± 0.01 nm difference between unannealed and B molecules. The height difference between unannealed molecules and the substrate is 0.63 ± 0.01 nm.

The earlier report[12] alludes to but does not document the results of experiments dedicated to comparing annealed films and post-deposited C_{60} atop Ni. Here we have described such experiments atop Ni(111), the results of which indicate that B molecules appear to sit 0.8 Å higher than molecules atop unreconstructed Ni(111). Indeed, the results for ML coverage (shown in Figure 6) over several substrate steps, show that B molecules on one step are identical in height to D molecules on the step above. This suggests that B *and* D molecules are in an identical adsorption environment, which, as it derives from vacancy formation, suggests that *all molecules in an annealed film* sit atop the Kagome-reconstructed substrate lattice first identified by Pai *et al.* for adsorption atop Cu(111).[5] That is, D molecules sit in 7-atom vacancies, and the adatoms thus displaced form 12-atom rings surrounding the B-molecules, in which adjacent rings share atoms to produce the Kagome lattice. This situation is presented in Figure 8 (b). As this means all molecules enjoy enhanced coordination with the substrate, we may reasonably expect them to look different to molecules that have never been subjected to annealing. Furthermore, a difference due to enhanced coordination would be manifested as greater conductivity, leading to increased apparent height in STM images. In addition, the step edges seen in Figure 6 have become porous compared to the clean steps shown in Figure 1, supporting the idea of Ni transport beneath C_{60} molecules suggested by Lin *et al.*[12]

Molecules in the unannealed shell of a C_{60} island atop Co(0001) (Figure 7 (b)) appear identical to B molecules in the annealed core. Taking into consideration the general undu-

lating nature of the substrate surface, they appear at the same z-level, leading us to conclude that only D-molecules sit atop reconstructed substrate.

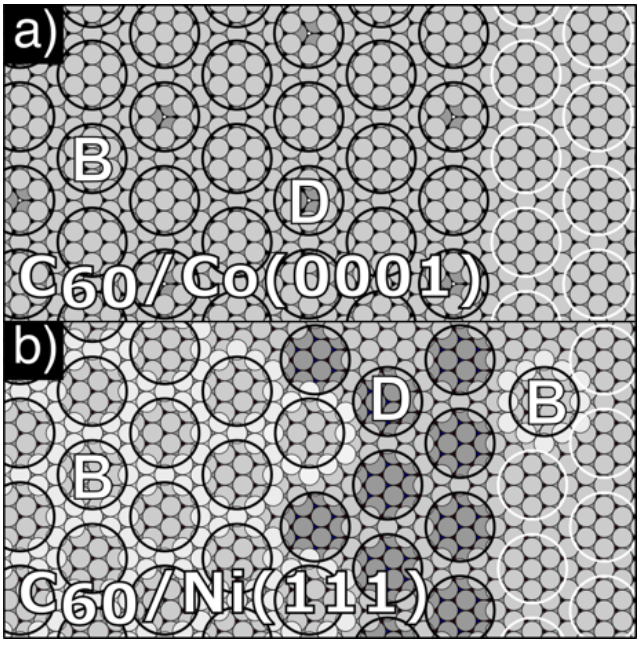

Figure 8: The models for annealed (4×4) C_{60} atop (a) Co(0001) and (b) Ni(111). (a) C_{60}/Co(0001). Bright (B) and dim (D) molecules are indicated. Molecules with a white outline show the unannealed situation for comparison.

From STM of the annealed film, it appears that the formation of a vacancy beneath one C_{60} acts to close off the possibility of vacancy formation beneath more than one or two adjacent C_{60}; indeed, observation of many images leads to the conclusion that it is not possible to form a contiguous 2d domain of vacancies of any size. Those rare situations in which a vacancy seems to be adjacent to another on all sides are always also associated with some surface feature, such as a step, a domain boundary, or a screw dislocation. No such restriction appears to be attached to B molecules, which form continuous lines and 2d domains connecting D molecules. The majority of molecules at the peripheries of islands are also B molecules.

Such a structure bears resemblance to 'buckled' structures observed on Al(111) and, after intermediate annealing, on Cu(111). Both these structures are associated with highly compressed C_{60} phases (on Al, NN=0.992 nm, on Cu, 0.965 nm), which the layer we observe

here is not (NN=1.0028 nm).

Conclusions

We have deposited C_{60} atop Ni(111) and Co(0001). LEED and STM show that the predominant domain orientation on both substrates is (4×4).

Other orientations are also present, before and after annealing. The most prevalent secondary phase, for both substrates, has C_{60} NN direction perpendicular to the (4×4) phase. High-resolution STM measurements were used to identify the most common adsorption configurations for C_{60}/Co(0001). We describe in detail a (7×7) phase for unannealed C_{60}/Co(0001), finding that the three C_{60} molecules in the unit cell occupy three distinct adsorption sites: two hollow sites with threefold symmetry and one atop site with sixfold symmetry. This is similar to the (7×7) C_{60}/Ni(111) phase observed by Picone *et al.*[17] In our measurements of C_{60}/Ni(111), identification of the molecular orientations was not possible. Due to the similar lattice parameters of Co(0001) and Ni(111), we conclude that the perpendicular orientation is (7×7) on both substrates.

In addition to the (4×4) and (7×7), we observe, in STM measurements, domains with other azimuthal relationships with the substrates, indicating HOC (higher order commensurate) ordering. These do not contribute to the LEED pattern.

The use of bulk Co is important, as it demonstrates that this surface is valid for surface science investigations, despite bringing significant experimental difficulties. We observe significant differences between adsorption on bulk Co (our study) and on a Co film on Au,[18] demonstrating the validity of independent investigations on bulk Co and the variety of behavior of surface phases dependent on subtle interplay between substrate and adsorbate. We present adoption of HOC structures as an alternative explanation to 'a highly strained Co film' as a solution to the conundrum of differing coexisting C_{60} phases.

We did not observe the metastable (7×7) C_{60}/Ni(111) structure observed by Picone *et*

al.[17] with STM; we attribute this to the metastability of the phase combined with differences in experimental conditions.

Post-annealing, both systems exhibit B and D (bright and dim) molecules. However, the details of this behavior differ profoundly per the substrate: on Co, the D molecules are mostly singletons in a semi-ordered arrangement, whereas on Ni, B molecules form islands surrounded by D molecules.

Annealed-core/unannealed-shell island experiments were used to show that on Ni, both B and D annealed molecules are in an identical adsorption environment which differs from that of an unannealed film and consists of the Kagome lattice identified for annealed C_{60}/Cu(111). This lattice is a (4×4) arrangement of hexagonal 7-atom substrate vacancies, one occupied by each C_{60} molecule.

In contrast, on Co(0001), similar experiments showed that B molecules in an annealed film had the same adsorption environment as an unannealed film. Line profile measurements on D molecules reveal that they adsorb on a reconstruction based on single-atom vacancies.

Neither system showed any significant dependence of the B and D populations on temperature or duration of annealing treatments, nor any evidence of vacancy diffusion.

We suggest that the important next step in this research avenue is the experimental observation of spin filtering in fullerene films on reconstructed magnetic surfaces.

Acknowledgments

This work was supported by the European EC-MetAC consortium. Data were processed using Gwyddion,[33] MATLAB[34] and Fiji.[35]

References

(1) Kroto, H. W.; Heath, J. R.; O'Brien, S. C.; Curl, R. F.; Smalley, R. E. C_{60}: Buckminsterfullerene. *Nature* **1985**, *318*, 162–163.

(2) Liu, T.; Troisi, A. What makes fullerene acceptors special as electron acceptors in organic solar cells and how to replace them. *Adv. Mat.* **2013**, *25*, 1038–1041.

(3) Shinohara, H. Endohedral metallofullerenes. *Rep. Progr. Phys.* **2000**, *63*, 843.

(4) Silien, C.; Pradhan, N. A.; Ho, W.; Thiry, P. A. Influence of adsorbate-substrate interaction on the local electronic structure of C_{60} studied by low-temperature STM. *Phys. Rev. B* **2004**, *69*, 115434.

(5) Pai, W. W.; Jeng, H. T.; Lin, C.; Xiao, X.; Zhao, A.; Zhang, X.; Xu, G.; Shi, X.; Van Hove, M. A.; Hsue, C. S.; Tsuei, K. D. Optimal Electron Doping of a C_{60} Monolayer on Cu(111) via Interface Reconstruction. *Phys. Rev. Lett.* **2010**, *104*, 036103.

(6) Shi, X.-Q.; Van Hove, M. A.; Zhang, R.-Q. Survey of structural and electronic properties of C_{60} on close-packed metal surfaces. *J. Mat. Sci.* **2012**, *47*, 7341–7355.

(7) Pussi, K.; Li, H.-I.; Shin, H.; Serkovic Loli, L. N. S.; Shukla, A. K.; Ledieu, J.; Fournée, V.; Wang, L. L.; Su, S. Y.; Marino, K. E.; Snyder, M. V.; Diehl, R. D. Elucidating the dynamical equilibrium of C_{60} molecules on Ag (111). *Phys. Rev. B* **2012**, *86*, 205406.

(8) Li, H.-I.; Pussi, K.; Hanna, K. J.; Wang, L.-L.; Johnson, D. D.; Cheng, H.-P.; Shin, H.; Curtarolo, S.; Moritz, W.; Smerdon, J. A.; McGrath, R.; Diehl, R. D. Surface geometry of C_{60} on Ag (111). *Phys. Rev. Lett.* **2009**, *103*, 056101.

(9) Shin, H.; Schwarze, A.; Diehl, R. D.; Pussi, K.; Colombier, A.; Gaudry, É.; Ledieu, J.; McGuirk, G. M.; Serkovic Loli, L. N.; Fournée, V.; Wang, L. L.; Schull, G.; Berndt, R. Structure and dynamics of C_{60} molecules on Au (111). *Phys. Rev. B* **2014**, *89*, 245428.

(10) Pai, W. W.; Hsu, C.-L.; Lin, M.; Lin, K.; Tang, T. Structural relaxation of adlayers in the presence of adsorbate-induced reconstruction: C_{60}/Cu(111). *Phys. Rev. B* **2004**, *69*, 125405.

(11) Pai, W. W.; Hsu, C.-L.; Chiang, C. R.; Chang, Y.; Lin, K. C. Origin of peculiar STM molecular contrast in C_{60}/Ag (100). *Surf. Sci.* **2002**, *519*, L605–L610.

(12) Lin, C. H.; Lin, K. C.; Tang, T. B.; Pai, W. W. Anomalous Surface Diffusion of C_{60} and Anisotropic Growth of Nano Islands on Ni (111). *J. Nanosci. Nanotech.* **2008**, *8*, 602–607.

(13) Pang, R.; Shi, X.; Van Hove, M. A. Manipulating magnetism at organic/ferromagnetic interfaces by molecule-induced surface reconstruction. *J. Am. Chem. Soc.* **2016**, *138*, 4029–4035.

(14) Kiguchi, M.; Iizumi, K.; Saiki, K.; Koma, A. Atomic and electronic structures of heteroepitaxial C_{60} film grown on Ni(111), Cu(111). *Appl. Surf. Sci.* **2003**, *212-213*, 101–104.

(15) Smerdon, J. A.; Giebink, N. C.; Guisinger, N. P.; Darancet, P.; Guest, J. R. Large Spatially Resolved Rectification in a Donor–Acceptor Molecular Heterojunction. *Nano Lett.* **2016**, *16*, 2603–2607.

(16) Smerdon, J. A.; Darancet, P.; Guest, J. R. Spatially resolved, substrate-induced rectification in C_{60} bilayers on copper. *J. Chem. Phys.* **2017**, *146*, 092328.

(17) Picone, A.; Finazzi, M.; Duò, L.; Giannotti, D.; Ciccacci, F.; Brambilla, A. Observation of a Metastable Honeycomb Arrangement of C_{60} on Ni(111) with (7×7) Periodicity: Tailoring an Interface for Organic Spintronics. *ACS Appl. Nano Mater.* **2021**, *4*, 12993–13000.

(18) Kollamana, J.; Wei, Z.; Laux, M.; Stöckl, J.; Stadtmüller, B.; Cinchetti, M.; Aeschlimann, M. Scanning Tunneling Microscopy Study of Ordered C_{60} Submonolayer Films on Co/Au(111). *J. Phys. Chem. C* **2016**, *120*, 7568–7574.

(19) Barbieri, A.; Van Hove, M.

(20) Shi, X.; Pang, A.; Man, K.; Zhang, R.; Minot, C.; Altman, M. S.; Van Hove, M. A. C_{60} on the Pt (111) surface: Structural tuning of electronic properties. *Phys. Rev. B* **2011**, *84*, 235406.

(21) Maxwell, A.; Brühwiler, P.; Arvanitis, D.; Hasselström, J.; Johansson, M.-J.; Mårtensson, N. Electronic and geometric structure of C_{60} on Al (111) and Al (110). *Phys. Rev. B* **1998**, *57*, 7312.

(22) Altman, E. I.; Colton, R. J. Determination of the orientation of C_{60} adsorbed on Au (111) and Ag (111). *Phys. Rev. B* **1993**, *48*, 18244.

(23) Felici, R.; Pedio, M.; Borgatti, F.; Iannotta, S.; Capozi, M.; Ciullo, G.; Stierle, A. X-ray-diffraction characterization of Pt (111) surface nanopatterning induced by C_{60} adsorption. *Nature Mat.* **2005**, *4*, 688–692.

(24) Li, H.; Franke, K.; Pascual, J.; Bruch, L.; Diehl, R. Origin of moiré structures in C_{60} on pb (111) and their effect on molecular energy levels. *Phys. Rev. B* **2009**, *80*, 085415.

(25) Schull, G.; Berndt, R. Orientationally ordered (7× 7) superstructure of C_{60} on Au (111). *Phys. Rev. Lett.* **2007**, *99*, 226105.

(26) Li, H.; Pussi, K.; Hanna, K.; Wang, L. L.; Johnson, D.; Cheng, H. P.; Shin, H.; Curtarolo, S.; Moritz, W.; Smerdon, J. A.; McGrath, R.; Diehl, R. D. Surface Geometry of C_{60} on Ag(111). *Phys. Rev. Lett.* **2009**, *103*, 056101.

(27) Shang, Y.; Wang, Z.; Yang, D.; Wang, Y.; Ma, C.; Tao, M.; Sun, K.; Yang, J.; Wang, J. Orientation ordering and chiral superstructures in fullerene monolayer on Cd (0001). *Nanomaterials* **2020**, *10*, 1305.

(28) David, W. I.; Ibberson, R. M.; Dennis, T. J. S.; Hare, J. P.; Prassides, K. Structural phase transitions in the fullerene C_{60}. *Europhys. Lett.* **1992**, *18*, 219.

(29) Tkatchenko, A. Commensurate monolayers on surfaces: geometry and ground states. *Phys. Rev. B* **2007**, *75*, 235411.

(30) Lagoute, J.; Kanisawa, K.; Fölsch, S. Manipulation and adsorption-site mapping of single pentacene molecules on Cu (111). *Phys. Rev. B* **2004**, *70*, 245415.

(31) Sakurai, T.; Wang, X. D.; Hashizume, T.; Yurov, V.; Shinohara, H.; Pickering, H. Adsorption of fullerenes on Cu (111) and Ag (111) surfaces. *Appl. Surf. Sci.* **1995**, *87*, 405–413.

(32) Haag, N.; Laux, M.; Stöckl, J.; Kollamana, J.; Seidel, J.; Großmann, N.; Fetzer, R.; Kelly, L. L.; Wei, Z.; Stadtmüller, B.; Cinchetti, M.; Aeschlimann, M. Epitaxial growth of thermally stable cobalt films on Au (111). *New J. Phys.* **2016**, *18*, 103054.

(33) Nečas, D.; Klapetek, P. Gwyddion: an open-source software for SPM data analysis. *Cent. Eur. J. Phys.* **2012**, *10*, 181–188.

(34) MATLAB, *9.7.0.1190202 (R2019b)*; The MathWorks Inc.: Natick, Massachusetts, 2018.

(35) Schindelin, J. et al. Fiji: an open-source platform for biological-image analysis. *Nature Methods* **2012**, *9*, 676–682.

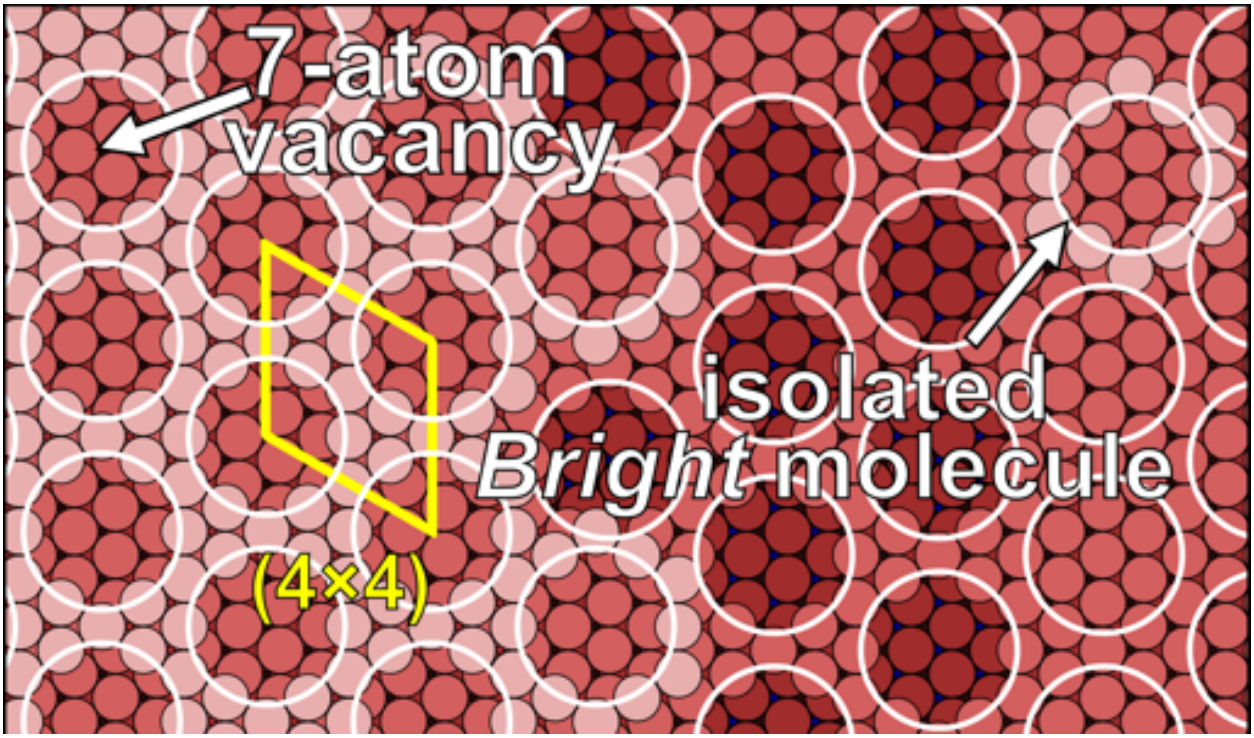

Figure 9: TOC image showing adsorption sites for fullerenes atop partially reconstructed Ni(111).